COMPRESSIVE BEHAVIOR OF CONCRETE-FILLED FRP TUBE COLUMNS: ASSESSMENT OF CRITICAL COLUMN PARAMETERS

Togay OZBAKKALOGLU*

ABSTRACT

A comprehensive experimental program has been underway at the Structures Laboratory of the University of Adelaide to investigate the behavior of concrete-filled fiber-reinforced polymer (FRP) tubes (CFFTs) under concentric compression. This paper presents the results from a group of 92 selected circular, square, and rectangular CFFTs and discusses the influence of the critical column parameters on the compressive behavior of CFFTs. These parameters include concrete strength, amount and type of FRP tube material, manufacture method of the tubes, and size and shape of the CFFTs. In addition to conventional FRP tubes, new types of tubes with integrated internal FRP reinforcement have been designed and tested. Results indicate that concrete strength, cross-sectional shape, and the amount and type of tube material significantly affect the behavior of CFFTs. The manufacture method of FRP tube also has some, but less significant, influence on the behavior of CFFTs. The influence of specimen size has been found to be small. No apparent difference has been found between the compressive behaviors of circular CFFTs and companion FRP-wrapped cylinders. The results also indicate that newly developed square and rectangular CFFTs, with internal FRP reinforcement, exhibit significantly improved behavior over conventional CFFTs.

KEYWORDS: Fiber reinforced polymers (FRP); Concrete; High-strength concrete; Columns; Confinement; Compressive behavior; Concrete-filled FRP tubes (CFFTs); Stress-strain relations.

* Senior Lecturer, School of Civil, Environmental and Engineering, University of Adelaide, Australia. Tel : + 618 8303 6477; Fax : +618 8303 4359; Email: tozbakka@civeng.adelaide.edu.au

INTRODUCTION

Over the past two decades the use of externally bonded fiber reinforced polymers (FRP) for strengthening reinforced concrete members has become widely accepted. As an important application of FRP composites, confinement of existing reinforced concrete columns with FRP jackets has been investigated extensively [1]. More recently, attention has turned to the potential applications of FRP composites for new structures. One such application, the concrete-filled FRP tube (CFFT), have received much attention and significant amount of research has been undertaken to investigate several aspects of structural performance of this composite system (e.g. [2-7]). Existing studies have demonstrated the ability of CFFTs to develop very high inelastic deformation capacities [4, 5, 8-11] making them an attractive alternative for the construction of earthquake-resistant high-performance columns.

It is well understood that lateral confinement can enhance both the strength and ductility of concrete. CFFTs owe their improved deformation capacities to the confinement action provided by the surrounding FRP tube. Therefore, to develop a rational procedure for designing CFFTs for use as earthquake-resistant columns in new construction, it is necessary to understand and be able to model the effects of FRP confinement on the stress-strain behavior of concrete in CFFTs. This requires a comprehensive investigation on the behavior of CFFTs under concentric compression. Although a number of such studies have been reported in the literature (e.g., [6, 12-14]), several aspects of CFFTs remain poorly understood and require more study. These include (i) high-strength concrete-filled FRP tubes (HSCFFTs), (ii) size effects on CFFTs, (iii) effects of FRP tube material and manufacture method, and (iv) confinement effectiveness of square and rectangular CFFTs.

Very much like that of FRP, the popularity of high-strength concrete (HSC) in the construction industry has been on a steady incline during the last two decades. It is now understood that HSC

offers superior performance and economy over normal-strength concrete (NSC) when used in the construction of bridges and multi-story buildings. The use of HSC for CFFTs is attractive because the combination of two high-strength materials (i.e., HSC and FRP) leads to high-performance columns. However, research on the compressive behavior of FRP-confined HSC, in general, and on HSCFFT, in particular, has so far been extremely limited, with only a few studies reported in the literature on FRP-wrapped concrete specimens [15-24].

Small specimens have been the focus of existing research on the compressive behavior of FRP-confined concrete; only limited data are available on realistically sized columns. Therefore, it is important to study the effects of size on the behavior of CFFTs to determine if and how test data on small specimens can be transferred to full-scale columns.

Research on CFFTs has mainly focused on two types of fibers (i.e., carbon and glass) as tube materials. Little research exists on CFFTs with tubes made of high-modulus (HM) carbon or aramid fibers. But the behavior of CFFTs is significantly influenced by the properties of the fibers used to manufacture them, and a certain fiber type could be more suitable for meeting design specifications in a given application. Therefore, for optimum design of CFFTs, it is important to understand the influence of fiber properties on the behavior of CFFTs.

Square and rectangular columns are extensively used in reinforced concrete structures. However, it is now well understood that square and rectangular tubes provide less effective confinement than circular tubes. Therefore, for similar levels of performance, square and rectangular CFFTs require more confinement, and hence more fibers in their tubes, than circular CFFTs. This could lead to significantly increased construction costs. However, early research has shown that the confinement effectiveness of square and rectangular tubes can be improved through alternative tube designs introduced by the author [25, 26]. Further research is

needed to fully investigate the influence of various tube arrangements on the confinement effectiveness of square and rectangular CFFTs.

These several aspects of CFFTs formed the focus of the research reported in this paper.

EXPERIMENTAL PROGRAM

Over 250 circular, square, and rectangular CFFTs have been manufactured and tested under concentric compression as part of an ongoing investigation at The University of Adelaide on FRP-concrete composite columns. This paper reports on the results from 92 of these CFFTs that were selected in order to critically assess the influence of the key column parameters on the compressive behavior of CFFTs. Specimens were divided into two major groups: (a) circular CFFTs and (b) square and rectangular CFFTs. In studies of the circular group, the influence of specimen size, concrete strength, tube material, and manufacture method on the compressive behavior of CFFTs was investigated. Furthermore, to establish relative performance of circular CFFTs with respect to FRP-wrapped concrete cylinders a group of companion FRP-wrapped specimens were also tested as part of the program. In studies of the square and rectangular group, the influence of concrete strength and key geometric properties on confinement effectiveness was investigated, and performance of new CFFT systems that were introduced by the author in attempts to improve confinement effectiveness were examined and compared with conventional CFFTs.

Test Specimens and Materials

All circular CFFTs were designed to have a height-to-diameter ratio (*H/D*) of two. The specimen diameter varied from 75 to 300 mm with the majority of the specimens having a diameter of 100 mm or 150 mm. For most of the circular CFFTs three nominally identical specimens were tested for each unique specimen configuration. Figure 1 shows typical circular CFFTs. Square and

rectangular CFFTs had a height of either 300 mm or 600 mm. HSC and UHSC FFTs were 300 mm in height and had either a 150 mm square or 113 x 225 mm rectangular cross-section, whereas NSCFFTs were 600 mm in height and had either a 200 mm square or 150 x 300 mm rectangular cross-section. The square CFFTs had a corner radius to sectional width ratio (*r/b*) of 0.2. Rectangular CFFTs of each series were manufactured with two different corner radii. The first group was provided with the same radius-corners with the companion square CFFTs and the CFFTs of the second group had one half of the corner radius of the specimens of the first group. Two nominally identical specimens were tested for each unique specimen configuration of HSC and UHSC FFTs, and a single specimen was tested for each NSCFFT configuration.

The FRP tubes of all square and the majority of circular CFFTs were manufactured using a manual wet lay-up process by wrapping epoxy resin impregnated fiber sheets around precision-cut high-density Styrofoam templates in the hoop direction. The square and rectangular tubes were prepared using unidirectional carbon fiber sheets, and the circular tubes were made using carbon, HM carbon, or aramid unidirectional fiber sheets. The carbon FRP (CFRP) tubes of HSC and UHSC square and rectangular CFFTs were manufactured using 0.234 mm thick carbon fiber sheets, and the tubes of all the remaining CFRP-confined CFFTs were prepared using a 0.117 mm thick version of the same fiber sheets. Figure 2 shows typical square and rectangular CFFTs before concrete casting. A group of circular CFFTs were designed with aramid FRP (AFRP) tubes that were manufactured using automated filament winding (FW) process with the majority of the fibers aligned along the hoop direction through the use of a winding angle of 88 degrees. Properties of the fibers used in the manufacture of the FRP tubes are shown in Table 1. The test results from the FRP coupon specimens prepared using the 0.117 mm thick carbon fiber sheets were previously reported in Ref.[25], and they are in close agreement with the coresponding fiber properties given in Table 1. In addition to conventional square and rectangular CFFTs, two new CFFT systems recently introduced by the author were also manufactured. The tubes of these

CFFTs were fitted with internal transverse FRP reinforcement, which was provided in the form of an FRP panel, in the case of rectangular CFFTs (Figure 2(c)), and in the form of FRP tubes, in the case of the square CFFT (Figure 2(d)). Further information on the manufacturing process of these CFFTs can be found elsewhere [25,26].

The specimens were prepared using three different grades of concrete, namely normal-strength concrete (NSC), high-strength concrete (HSC) and ultra high-strength concrete (UHSC). In this paper, unconfined concrete strengths (f'_{co}) below 55 MPa is referred to as NSC, between 55 MPa and 100 MPa as HSC and over 100 MPa as UHSC. In designing the FRP tubes, due consideration was given to the well-understood influence of the strength of concrete on its confinement demand [5, 24]. This was done through the use of nominal confinement ratio f_l/f'_{co}, calculated from Eq.1 assuming a uniform confinement distribution, as the performance criterion in establishing relative confinement levels of CFFTs with different diameters and concrete strengths.

$$\frac{f_l}{f'_{co}} = \frac{2E_f t_f \varepsilon_f}{Df'_{co}} \quad (1)$$

where, f_l is the confining pressure, E_f is the modulus of elasticity, t_f is the total nominal thickness and ε_f is the ultimate tensile strain of the fibers, and D is the internal diameter of the CFFT.

Specimen Designation

The circular CFFTs in Tables 2 to 6 and Figures 5 to 10 were labeled as follows: the letters N, H and UH were used to label NSC, HSC and UHSC. This was followed by a number that indicated the nominal diameter of the CFFT. The type and number of layers of FRP used in the CFFT were given next, with A, C and HMC standing for aramid, carbon and HM carbon FRP, respectively. For the filament wound specimens the letter that indicated the FRP type was followed by an acronym FW. For the FRP-wrapped specimens the specimen designation included a final letter W that followed the number that indicated the number of FRP layers. The square and rectangular

CFFTs in Tables 7 to 10 and Figures 12 to 15 were labeled as follows: letters S and R were used for labeling square and rectangular CFFT, which was followed by letters N, H or UH were used to indicate NSC, HSC or UHSC. In the case of conventional CFFTs, these were followed by a number that was used to make a distinction between the CFFTs that had a different level of confinement and/or corner radius. For the special CFFT systems the letter used to indicate the concrete strength was followed by the final acronyms of IP, RIP or IT to indicate internal panel, rounded internal panel or internal tube.

Instrumentation and testing

Axial deformations of the CFFTs were measured with four linear variable displacement transducers (LVDTs), which were mounted at the corners between the loading and supporting steel plates of the test machine, as shown in Fig. 3. Deformation readings were used to calculate average axial strains along the heights of the specimens. In addition, axial and transverse strains were measured by a large number of unidirectional strain gauges, which were installed at critical locations on the tubes.

The specimens were tested under monotonically increasing axial compression, using a 5000-kN capacity universal testing machine. Prior to testing, both ends of all specimens were capped to ensure the applied pressure was uniformly distributed, and the load was applied directly to the concrete core through the use of precision-cut steel plates. The test setup and instrumentation are shown in Fig. 3.

TEST RESULTS AND DISCUSSION

Circular CFFTs

In this section, first the failure modes observed in circular CFFTs are described; the influence of size, concrete strength, tube material, manufacture method, and confinement technique on axial stress-strain relations and ultimate condition of circular CFFTs is then discussed. The ultimate

condition of FRP-confined concrete is defined as the ultimate strength f'_{cc} and axial strain ε_{cu} of concrete measured at the failure of the specimen at the recorded hoop rupture strain $\varepsilon_{h,rup}$. These key values are reported together with material and geometric properties for all circular CFFTs in Tables 2 to 6.

Failure modes

Typical failures of the circular CFFTs are shown in Fig. 4. In all specimens, failure resulted from a rupture of the FRP tube. Figure 4 highlights the differences between the failure modes of NSC and UHSC FFTs. In UHSCFFTs, damage was localized around a single major crack without any significant damage in the rest of the section. But in NSCFFTs, damage in the concrete was more evenly distributed, implying that a large portion of concrete at the critical section crushed gradually before the FRP tube ruptured.

Axial stress-strain behavior and ultimate condition

Representative axial stress-strain curves for the circular CFFTs are shown in Figs. 5 to 10, and the summary of the key experimental results are given in Tables 2 to 6, which include: ultimate axial strength and strain (f'_{cc} *and* ε_{cu}), strength and strain enhancement ratios (f'_{cc}/f'_{co} *and* $\varepsilon_{cu}/\varepsilon_{co}$) and FRP hoop rupture strain ($\varepsilon_{h,rup.}$). In most cases the values reported in Tables 2 to 6 were averaged from three nominally identical specimens. The hoop rupture strains $\varepsilon_{h,rupt}$ reported in the tables were averaged from at least three strain gauge readings that were placed outside the overlap region and ε_{co} values were calculated using the expression given by Popovics [27]. Figures 5-10 and Tables 2-6 illustrate the influence of important column parameters on the compressive behavior of CFFTs.

<u>Influence of specimen size</u>

Figure 5 illustrates the stress-strain behavior of three groups of circular CFFTs. Table 2 provides material, geometric and ultimate condition properties of these specimens. The CFFTs of each group were manufactured using the same concrete mix and they were confined with the same FRP material. As can be seen in Table 2 the unconfined concrete strengths (f'_{co}) varied slightly in each group due to the influences of the specimen size and age of concrete by the time of testing. The nominal confinement ratios f_l/f'_{co} of the CFFTs of each group were reasonably close, on the other hand, allowing a meaningful comparison. The NSCFFTs shown in Fig. 5(a) were all confined by CFRP and had a diameter of 75, 150 or 300 mm. It is evident from the figure that the 75- and 150-mm diameter CFFTs exhibited almost identical behavior with the 300-mm diameter CFFT developing a slightly lower strength enhancement (f'_{cc}/f'_{co}). Figures 5(b) and 5(c) and corresponding specimen groups in Table 2 show the results from AFRP confined HSC and UHSC FFTs, respectively. From the comparison of the stress-train curves shown in these figures and results reported in the table it is clear that specimen size has no major influence on the compressive behavior of circular CFFTs within the size range investigated in the present study. This observation is in agreement with those previously reported on FRP-wrapped NSC cylinders [28,29].

Influence of concrete strength

Each of the four sets of stress-strain curves shown in Fig. 6 were arranged to illustrate the influence of concrete strength on the axial behavior of circular CFFTs. Table 3 provide the important properties of the CFFTs shown in Fig. 6. A number of important observations can be made based on the results shown in these figure and tables. The results indicate that for a given nominal confinement ratio f_l/f'_{co} the strength enhancement ratio f'_{cc}/f'_{co} of CFFTs decrease with an increase in unconfined concrete strength (f'_{co}). As can be seen in Table 3, a similar trend is also present for the strain enhancement ratio ($\varepsilon_{cu}/\varepsilon_{co}$), although the ultimate axial strains of the CFFTs were not influenced significantly by the concrete strength especially in AFRP made

CFFTs as evident from Fig. 6. The results further illustrate that an increase in concrete strength leads to a decrease in the hoop rupture strain ($\varepsilon_{h,rup}$) and resulting strain reduction factor (k_ε)

$$k_\varepsilon = \frac{\varepsilon_{h,rup}}{\varepsilon_f} \quad (2)$$

The influence of the concrete strength on the strain reduction factor k_ε was first discussed in Ozbakkaloglu and Akin [24] and the results of the present study are in agreement with the observations reported in that study. It is evident from the results shown in Table 3, there is a strong correlation between k_ε and f'_{co} in both AFRP and CFRP made CFFTs. However, this trend is not as clear for the CFFTs with filament wound tubes as it is for the CFFTs with manually manufactured tubes. Further research is required for an in-depth investigation of these important observations on the influence of concrete strength and tube manufacture method on the strain reduction factor k_ε.

For a closer inspection of the main behavioral influences that leads to lower strength enhancement ratios of higher strength CFFTs, the stress-strain curves of six 100-MPa 152mm-diameter CFFTs with one to six layers of CFRP are shown in Fig. 7. The figure illustrates that when the amount of confinement is below a certain threshold, HSCFFTs exhibit strain softening with limited improvement in compressive behavior. Four layers of CFRP were required for 100-MPa concrete to attain this threshold and hence to confine the concrete sufficiently. Hence, only the additional layers over the initial four layers provided enhancement in the concrete strength. Similar behavior is observed in NSCFFTs; however, the amount of confinement required to sufficiently confine concrete increases significantly with concrete strength. Nevertheless, the results of the present study clearly demonstrate that sufficiently confined HSC and UHSC FFTs can exhibit highly ductile behavior.

Influence of tube material

Figure 8 illustrates the influence of tube material on the axial stress-strain behavior of CFFTs through the comparison of representative stress-strain curves of CFFTs made using different types of FRP sheets. Table 4 provides the important properties of the CFFTs shown in Fig.8. The two CFFTs shown in Fig. 8 (a) were confined either with 5-layer CFRP or with 4-layer AFRP which gave them an almost identical nominal confinement ratios f_l/f'_{co}. A similar comparison is shown between 2-layer CFRP and HM CFRP confined CFFTs in Fig. 8(b). Figures 8(a) and 8(b) illustrate that all three CFFTs developed similar ultimate compressive strengths. However, it is evident from the figures that significant differences exist in the ultimate axial strain of the CFFTs, with AFRP-confined CFFT developing the highest ultimate strain and HM CFRP-confined CFFT developing the lowest. This comparison makes evident the significant correlation between the ultimate rupture strain of fibers and the ultimate axial strain of CFFTs manufactured using them.

Influence of tube manufacture method

Figure 9 shows representative stress-strain curves of two CFFT systems; one manufactured using a manual hand lay-up technique (Specimen H-100-A3) and the other using automated filament winding process (Specimen H-100-AFW). The average values of the key specimen properties and test results are shown in Table 5 for each CFFT system. Although, the properties of aramid fibers used in fabrication of these CFFT systems were slightly different, the two systems had identical nominal confinement ratios f_l/f'_{co}. Figure 9 and Table 5 illustrate that the CFFTs with tubes manufactured using filament winding process developed higher ultimate axial stress and strain. The longer second branch of Specimen H-100-AFW over Specimen H-100-A3 can be associated to the higher rupture strain of the former CFFT. On the other hand, the almost identical second branch slopes of the two CFFT systems suggest that the higher confinement effectiveness of the filament wound system appears to have contributed to the overall better performance of these CFFTs. That is, the higher tube stiffness of the hand lay-up CFFTs, caused by higher elastic modulus of their fibers, would have lead to a larger slope of the second branch if the confinement

effectiveness of the two systems were identical. The higher confinement effectiveness of the tubes manufactured using filament winding method was expected and can be attributed to better precision in fiber placement and better implementation of quality control measures. Nevertheless, this comparison demonstrates that the manual wet lay-up technique compares reasonably well with precision manufacturing methods of FRP tubes.

The average ultimate rupture strain of the filament wound CFFTs was also higher, yet when divided with the higher rupture strain of the fibers used in these tubes it yielded an almost identical strain reduction factor k_ε as the CFFTs manufactured using manual wet lay-up technique, as shown in Table 5.

Influence of confinement technique

To establish the relative performance of circular CFFTs with respect to FRP-wrapped concrete cylinders, representative stress-strain curves of a CFFT and a companion FRP-wrapped specimen are shown in Fig.10. Table 6 provides the material and geometric properties of these specimens as well as their experimentally obtained ultimate conditions. It is evident from both Fig. 10 and Table 6 that there is no perceptible difference between the compressive behavior of FRP-wrapped specimens and CFFTs, both groups developing almost the same ultimate axial stress, ultimate axial strain and hoop rupture strain. It should be noted, however, that the CFFTs of the present study were cured in the fog room until a few days before the time of testing, which took place around 7 weeks after concrete casting. Therefore, it was highly unlikely that the concrete in the CFFTs had developed significant volume shrinkage. It would be reasonable to expect, however, that CFFTs under different exposure durations and conditions may develop some shrinkage, which could affect the dilation behavior of the CFFT and in turn may result in some deviation in its compressive behavior over a comparable FRP-wrapped specimen. Apart from this long-term behavior consideration, however, the results reported herein illustrate that these two confinement

techniques provide almost an identical level of improvement on the compressive behavior of concrete. This observation renders the other factors that have been hypothesized in the literature to cause differences in the behavior of CFFTs and FRP-wrapped concrete unimportant.

Square and rectangular CFFTs

In this section, first the failure modes observed in square and rectangular CFFTs are described, the influences of concrete strength, corner radius and sectional aspect ratio on the stress-strain behavior of CFFTs are then discussed and their interactions with each other are outlined. Finally, performance of the new CFFT systems recently introduced by the author [25,26] in attempts to improve confinement effectiveness of square and rectangular CFFTs are examined and compared with conventional CFFTs.

Failure modes

Typical failures of the square and rectangular CFFTs are shown in Fig. 11. In all specimens, failure resulted from the rupture of the FRP tube. In CFFTs without internal FRP reinforcement, failure occurred at or near one of the corners of the CFFTs. As can be seen from Figs.11(a), 11(b) and 11(d), the CFFTs with higher confinement effectiveness (i.e., square CFFTs with well-rounded corners) had a much more global failure where the rupture of the FRP tube extended from top to bottom of the specimen. In the CFFTs with lower confinement effectiveness, on the other hand, the rupture of the FRP tube was more local and it was isolated to a smaller section along the height of the specimen (Figs. 11(c) and 11(e)). The failure modes of the CFFTs with internal FRP reinforcement were more complex because of the interactions between the internal FRP and the external tube. A detailed discussion on the failure modes of these CFFTs can be found elsewhere [25,26].

Axial stress-strain behavior and ultimate conditions

Representative axial stress-strain curves of square and rectangular CFFTs are shown in Figs. 12 to 15 and the summary of the key experimental results are given in Tables 7 to 10. These figures and tables illustrate the influence of important confinement parameters on the compressive behavior of CFFTs, as discussed in the following sections.

Influences of concrete strength, sectional aspect ratio and corner radius

Figures 12(a) and 12(b) show selected stress-train curves of the square CFFTs. In each figure the curves of NSC, HSC and UHSC CFFTs with relatively close nominal confinement ratios are shown. The averaged results of these CFFTs are given in Table 7. All square CFFTs had well-rounded corners with a corner radius to width ratio (r/b) of 0.2. NSC, HSC and UHSC CFFTs shown in Figures 12(a) and 12(b) were companion specimens, and the CFFTs of each series were identical except for their tube stiffness. The nominal confinement ratios of the CFFTs shown in Fig. 12(a) varied from 0.46 to 0.55, whereas the CFFTs shown in Fig. 12(b) had higher ratios that ranged between 0.77 and 0.86. Figure 12(a) illustrates that the confinement level that provided a strength enhancement for the NSC CFFT was just enough for the HSC and UHSC specimens to exhibit an almost flat/horizontal overall second branch trend. This observation is consistent with those derived from the investigation of the circular CFFTs as discussed previously. As evident from Fig.12(b) increasing the amount of confinement results in an increase in the ultimate axial stress and strain of all the CFFTs. It is clear from Table 7, however, that for a given nominal confinement ratio f_l/f'_{co} both the stress and strain enhancement ratios (f'_{cc}/f'_{co} and $\varepsilon_{cc}/\varepsilon_{co}$) decrease with an increase in concrete strength.

Figure 13 shows the selected stress-train curves of the rectangular CFFTs. The CFFTs shown in Figs. 13(a) and 13(b) all had a sectional aspect ratio of 2.0 and the specimens shown in each figure had the same corner radius to sectional dimension ratio and reasonably close nominal confinement ratios. The rectangular CFFTs shown in Fig. 13(a) were companion to the square

CFFTs shown in Fig. 12(b) and, for a given series, the only difference between the two groups was the sectional aspect ratio. NSC, HSC and UHSC FFTs shown in Figures 13(a) and 13(b) were companion specimens, and the CFFTs of each series were identical except for their corner radius. Table 8 summarizes the average results of the CFFTs shown in Figs. 13(a) and 13(b), respectively. The comparison of the curves shown in Fig.13(a) with those shown in Fig.12(b) and Fig.13(b), respectively, illustrate the well-understood influence of the sectional aspect ratio and corner radius on the compressive behavior of square and rectangular CFFTs. As has been reported previously for both FRP-wrapped concrete specimens [30-33] and CFFTs [6, 14] the confinement effectiveness of FRP jackets/tubes increases with an increase in corner radius and decreases with an increase in sectional aspect ratio over unity. These influences are directly evident from the above comparisons.

A closer inspection of the curves shown in Figs.13(a) and 13(b) leads to a number of interesting observations in regards to the combined influence of concrete strength and confinement effectiveness of the FRP tube. Figure 13(a) illustrates that both NSC and HSC FFTs with well-rounded corners exhibited almost continuously ascending stress-strain curves without any significant softening. The same figure shows, however, that UHSCFFT (Specimen RUH1) experienced major strength decay at the transition point of its stress-strain curve. This difference in behavior points to the sensitivity of higher-strength CFFTs to the effectiveness of confining tube. The increased sensitivity can be explained by the more sudden and brittle failure mode of HSC compared to the gradual failure mode of NSC, which exhibits a more pronounced softening behavior and in turn allows the gradual activation of the confinement mechanism.

This observation is further supported by the stress-strain curves shown in Fig. 13(b), which illustrate that both HSC and UHSC FFTs with smaller-radius corners experienced large strength decay just after attaining their initial peak strengths. This suggests that the lowered confinement

effectiveness of the rectangular tube with smaller-radius corners was no longer sufficient to prevent the strength loss in HSCFFTs. As discussed previously, the rectangular tube with well-rounded corners provided sufficiently high confinement effectiveness to prevent this loss in the HSCFFT but not in the UHSCFFT. As can be seen in Fig.12(b), none of the companion square CFFTs experienced a strength loss, suggesting that the confinement effectiveness of this system was high enough to prevent this even for the UHSCFFT. It is clear from the above discussion that the tubes with lower confinement effectiveness may not provide sufficient confinement to allow HSC and UHSC FFTs to maintain their load carrying capacity after their initial peak strengths are attained. Therefore, in the design and manufacture of these high-strength CFFT systems due consideration should be given to the confinement effectiveness of the confining tubes and efforts need to be made to develop and use forms with higher confinement effectiveness.

New CFFT systems

Rectangular CFFTs with internal FRP panels

Figure 14 shows the stress-strain curves for three rectangular CFFTs. These CFFTs were cast from the same batch of concrete and they had identical CFRP external tubes. Two of the CFFTs had internal panels that were manufactured using the same carbon fiber sheets that were used in the exterior tube. One of these special CFFTs (Specimen RN-RIP) was designed with a rounded internal panel-external tube connection (very much like the corners of the external tube) to reduce the stress concentrations experienced at these connections. The other internal panel CFFT (RN-IP) had a 90 degree internal panel-external tube connection.

The stress-strain curves shown in Fig. 14 and results reported in Table 9 indicate that incorporation of an internal panel leads to a significant improvement on both the ultimate strength f'_{cc} and axial strain ε_{cu} of rectangular CFFTs. As evident from Fig. 14, the overall trends of the second branches of the stress-strain curves were significantly influenced by the presence of an

internal panel, with both of the internal panel CFFTs exhibiting an ascending second branch compared to an almost flat second branch of the conventional rectangular CFFT (Specimen RN3). These observations indicate that the presence of an internal panel improves the compressive behavior of rectangular CFFTs through both increasing the confinement effectives of their tubes and delaying their rupture.

Comparison of the stress-strain curves of Specimens RN-IP and RN-RIP in Fig.14 illustrates the influence of the internal panel-external tube connection detail. Specimen RN-RIP with a rounded connection exhibits a stress-strain curve with a much more steeply ascending second branch compared to that of Specimen RN-IP with a 90 degree connection, indicating that the confinement effectiveness of the tubes with internal panels can be further increased through the use of rounded panel-tube connections.

Square CFFT made of concrete-filled FRP cylinders

Figure 15 shows the stress-strain curve for the tube-reinforced CFFT, Specimen SN-IT, together with that of a square CFFT, Specimen SN2, with no internal reinforcement. Both CFFTs were made from the same CFRP material and they had the same external dimensions and unconfined concrete strength. Specimens SN2 and SN-IT also had the same amount of fibers in their external tubes. Specimen SN-IT consisted of four 100mm-diameter circular internal tubes brought together in the arrangement shown in Fig. 2(d), giving a corner radius of 50 mm to the resulting external square tube. The corner radius of Specimen SN2 was 40 mm. Their similar material and geometric properties made the two specimens a suitable pair for comparison.

The stress-strain curves shown in Fig. 15 and results given in Table 10 illustrate the remarkable difference in the confinement effectiveness of these two CFFT systems. The ultimate compressive strength of the tube-reinforced CFFT was almost twice the strength of the

companion conventional CFFT. In fact, the stress-strain behavior of the tube-reinforced CFFT closely resembled that of circular CFFTs, which are known to have significantly higher confinement effectiveness than square and rectangular CFFTs.

CONCLUSIONS

This paper has presented a comprehensive assessment of the critical column parameters that influence the axial compressive behavior of circular, square and rectangular CFFTs. Based on the results and discussions reported in this paper, the following conclusions can be drawn.

1. For circular CFFTs, specimen size has only a slight influence on the compressive behavior of CFFTs with the ultimate axial strength and strain only slightly influenced by the size of CFFTs: small specimens exhibit slightly better performance than their larger counterparts. This is true within the range of parameters investigated in the present study and further research is needed to study various tube materials, concrete strengths and a wider range of specimen dimensions before more general conclusions can be drawn.

2. Sufficiently confined HSC and UHSC FFTs can exhibit highly ductile behavior. However, the amount of confinement required to sufficiently confine higher-strength CFFTs is higher than that required for normal-strength CFFTs. For a given nominal confinement ratio f_l/f'_{co}, higher-strength CFFTs develop lower strength and strain enhancement ratios (f'_{cc}/f'_{co} *and* $\varepsilon_{cu}/\varepsilon_{co}$) than normal-strength CFFTs.

3. Compressive behavior of CFFTs is significantly influenced by the mechanical properties of fibers used in their FRP tubes. A strong correlation exists between the ultimate rupture strain of fibers and the ultimate axial strain of CFFTs made using them.

4. FRP tubes manufactured using automated filament winding method provides a slightly more efficient confinement compared to tubes made using manual wet lay-up technique. It has been shown, however, that the resulting performance difference is not very significant.

5. There is no apparent difference between the compressive behaviors of CFFTs and companion FRP-wrapped concrete specimens when shrinkage of concrete is prevented in CFFTs. Further

research is needed to understand the influence of shrinkage on the dilation behavior of concrete in CFFTs and the resulting compressive behavior of CFFTs.

6. Compressive behavior of square and rectangular HSC and UHSC FFTs is highly sensitive to the effectiveness of confining tube, and tubes with low confinement effectiveness may not provide sufficient confinement to allow higher-strength CFFTs to maintain their load carrying capacity after their initial peak strengths are attained. Both the corner radius of the tube and the sectional aspect ratio significantly influence the compressive behavior of rectangular CFFTs, and the behavior improves as the corner radius increases and as the aspect ratio approaches unity.

7. Integration of internal FRP reinforcement into square and rectangular FRP tubes significantly increases the confinement effectiveness of the tubes, and CFFT systems manufactured using these tubes demonstrate substantially improved compressive behavior compared to conventional CFFTs.

ACKNOWLEDGEMENTS

The author would like to thank Drs. Cagri Ayranci and Pierre Mertini at the University of Alberta, who manufactured the tubes of the filament wound CFFTs reported in this paper.

REFERENCES

1. Ozbakkaloglu, T., Lim, J. C., and Vincent, T. (2012). “FRP-Confined Concrete in Circular Sections: Review and Assessment of Stress-Strain Models.” Engineering Structures, http://dx.doi.org/10.1016/j.engstruct.2012.06.010.
2. Mirmiran, A., Shahawy, M., Samaan, M., El Echary, H., Mastrapa, J.C., and Pico, O. (1998). “Effect of Column Parameters on FRP-confined Concrete.” Journal of Composites for Construction, ASCE, 2, 4, pp 175-185.
3. Fam, A. Z., and Rizkalla, S. H. (2002). “Flexural behavior of concrete-filled fiber reinforced polymer circular tubes.” *Journal of Composites for Construction*, 6(2), 123-132.

4. Ozbakkaloglu, T., and Saatcioglu, M. (2006). “Seismic behavior of high-strength concrete Columns confined by fiber reinforced polymer tubes.” *Journal of Composites for Construction, ASCE*, 10(6), 538-549.
5. Ozbakkaloglu, T., and Saatcioglu, M. (2007). “Seismic performance of square high-strength concrete columns in FRP stay-in-place formwork.” *Journal of Structural Engineering, ASCE*, 133(1), 44-56.
6. Ozbakkaloglu, T., and Oehlers, D. J. (2008). “Concrete-filled Square and Rectangular FRP Tubes under Axial Compression.” Journal of Composites for Construction, ASCE, Vol.12, No.4, pp.469-477.
7. Zaghi, A.E., Saiidi, M.S., and Mirmiran, A. (2012). “Shake table response and analysis of a concrete-filled FRP tube bridge column.” Composite Structures, 94 (5), 164-1574.
8. Seible, F., Burgueño, R., Abdallah, M.G., and Nuismer, R. (1996). “Development of advanced composite carbon shell systems for concrete columns in seismic zones.” Proceedings of the 11th World Conference on Earthquake Engineering, Elsevier Science, Paper No. 1375.
9. Zhou, W., Fan, L., and Xue, Y. (2001). “Shaking table testing of simply supported bridges with prefabricated GFRP tube jacketed RC columns.” Proceedings of the International Conference on FRP Composites in Civil Engineering, Hong Kong, Vol. II, pp 1337-1344.
10. Yamakawa, T., Zhong, P., and Ohama, A. (2003). “Seismic Performance of Aramid Fiber Square Tubed Concrete Columns with Metallic and/or Non-metallic Reinforcement” Journal of Reinforced Plastics and Composites, 22, 13, pp 1221-1237.
11. Shao, Y., and Mirmiran, A. (2005). “Experimental Investigation of Cyclic Behavior of Concrete-Filled FRP Tubes,” Journal of Composites for Construction, ASCE, 9(3), 263-273.
12. Li., G. (2006). “Experimental study of FRP confined concrete cylinders.” Engineering Structures, Vol. 28, pp 1001-1008.
13. Mohamed, H., and Masmoudi, R. (2010) “Axial Load Capacity of Concrete-Filled FRP Tube Columns: Experimental versus Predictions.” J. Compos. Constr., ASCE, 14(2): p. 231-243.

14. Ozbakkaloglu, T. (2012). “Axial Compressive Behavior of Square and Rectangular High-Strength Concrete-Filled FRP Tubes.” Journal of Composites for Construction, ASCE, doi: 10.1061/(ASCE)CC.1943-5614.0000321
15. Rousakis, T.C. (2001). “Experimental investigation of concrete cylinders confined by carbon FRP sheets under monotonic and cyclic axial compression load.” *Research Report 01:2*, Division of Building Technology, Chalmers University of Technology.
16. Berthet, J. F., Ferrier, E., and Hamelin, P. (2005). “Compressive behaviour of concrete externally confined by composite jackets. Part A: Experimental study.” *Construction and Building Materials, Elsevie*r, 19, 223-232.
17. Mandal., S., Hoskin., A., and Fam., A. (2005). “Influence of Concrete Strength on Confinement Effectiveness of Fiber-Reinforced Polymer Circular Jackets.” ACI Structural Journal, 102, 3, pp 383-392.
18. Almusallam, T. H. (2007). “Behaviour of normal and high-strength concrete cylinders confined with E-Glass/Epoxy composite laminates.” *Composites Part B-Engineering*, 38(5-6), 629-639.
19. Eid, R., Roy, N., and Paultre, P. (2009). “Normal- and high-strength concrete circular elements wrapped with FRP composites.” Journal of Composites for Construction, ASCE, 13(2), 113-124.
20. Wu, H. L., Wang, Y. F., Yu, L., and Li, X. R. (2009). “Experimental and computational studies on high-strength concrete circular columns confined by aramid fiber-reinforced polymer sheets.” *Journal of Composites for Construction, ASCE*, 13(2), 125-134.
21. Cui, C., and Sheikh, S.A. (2010). “Experimental study of normal- and high-strength concrete confined with fiber-reinforced polymers.” *Journal of Composites for Construction, ASCE*, 14(5), 553-561.
22. Wang, Y.F., and Wu, H.L. (2010). “Experimental investigation on square high-strength concrete short columns confined with AFRP sheets.” J Compos Constr, ASCE; 14(3): 346–51.
23. Xiao, Q. G., Teng, J. G., and Yu, T. (2010). “Behavior and modeling of confined high-strength concrete.” *Journal of Composites for Construction, ASCE*, 14(3), 249-259.

24. Ozbakkaloglu, T., and Akin, E. (2012) “Behavior of FRP-confined normal- and high-strength concrete under cyclic axial compression.” Journal of Composites for Construction, ASCE, 16(4), 451-463.
25. Ozbakkaloglu, T. and Oehlers, D. J. (2008). “Manufacture and testing of a novel FRP tube confinement system.” *Engineering Structures*, 30, 2448-2459.
26. Ozbakkaloglu, T. (2012). “Concrete-filled FRP Tubes: Manufacture and Testing of New Forms Designed for Improved Performance.” Journal of Composites for Construction, ASCE, doi: 10.1061/(ASCE)CC.1943-5614.0000334
27. Popovics S. (1973). “Numerical approach to the complete stress-strain relation for concrete.” Cem Concr Res; 3(5): 583-99.
28. Wang, Y.F., and Wu, H.L. (2011). “Size Effect of Concrete Short Columns Confined with Aramid FRP Jackets.” *Journal of Composites for Construction, ASCE*, 15(4), 535-544.
29. Liang, M., Wu, Z.M., Ueda, T., Zheng, J.J., and Akogbe, R. (2012). “Experiment and modeling on axial behavior of carbon fiber reinforced polymer confined concrete cylinders with different sizes.” Journal of Reinforced Plastics and Composites, 31(6), pp 389-403.
30. Rochette, P., and Labossiere, P. (2000). “Axial Testing of Rectangular Column Models Confined with Composites.” Journal of Composites for Construction, ASCE, 4, 3, pp 129-136.
31. Lam, L., and Teng, J.G. (2003). “Design-oriented stress-strain model for FRP-confined concrete in rectangular columns.” Journal of Reinforced Plastics and Composites, 22(13), pp 1149-1186.
32. Wang, L. M., and Wu, Y. F. (2008). “Effect of Corner Radius on the Performance of CFRP-Confined Square Concrete Columns: Test.” *Engineering Structures,* 30(2): p. 493-505.
33. Wu Y.F., and Wei Y.Y. (2010). “Effect of cross-sectional aspect ratio on the strength of CFRP-confined rectangular concrete columns.” *Engineering Structures*, 32: 32-45.

Table 1. Fiber properties as reported by the manufacturers

Type	Nominal thickness t_f (mm/ply)	Tensile strength f_f (MPa)	Ultimate tensile strain, ε_f (%)	Elastic modulus E_f (GPa)
Carbon1	0.117	3800	1.55	240
Carbon2	0.234	3800	1.55	240
HM Carbon	0.190	2650	0.40	640
Aramid	0.200	2900	2.50	120
Aramid-FW	-	2930	2.90	99

Table 2. Influence of specimen size on compressive behavior of circular CFFTs

Group	Specimen	f'_{co} (MPa)	D (mm)	H (mm)	FRP type	FRP layers	f_l/f'_{co}	f'_{cc} (MPa)	f'_{cc}/f'_{co}	ε_{cu} (%)	$\varepsilon_{cu}/\varepsilon_{co}$	$\varepsilon_{h,rup}$ (%)	k_ε
NSC CFRP	N-75-C1	43.0	74	150	CFRP1	1	0.28	69.2	1.61	1.40	5.8	1.20	0.77
	N-150-C2	36.4	152	305	CFRP1	2	0.32	60.6	1.67	1.47	6.4	1.30	0.84
	N-300-C4	36.3	302	605	CFRP1	4	0.32	57.0	1.57	1.52	6.6	1.17	0.75
HSC AFRP	H-100-A2	83.6	100	200	AFRP	2	0.28	113.6	1.36	1.63	5.7	1.84	0.74
	H-150-A3	77.9	152	305	AFRP	3	0.29	108.3	1.39	1.85	6.6	1.83	0.73
UHSC AFRP	UH-100-A4	110.1	100	200	AFRP	4	0.42	187.4	1.70	2.34	7.7	1.52	0.61
	UH-150-A6	104.5	152	305	AFRP	6	0.44	173.8	1.66	2.12	7.1	1.58	0.63

Table 3. Influence of concrete strength on compressive behavior of circular CFFTs

Group	Specimen	f'_{co} (MPa)	D (mm)	H (mm)	FRP type	FRP layers	f_l/f'_{co}	f'_{cc} (MPa)	f'_{cc}/f'_{co}	ε_{cu} (%)	$\varepsilon_{cu}/\varepsilon_{co}$	$\varepsilon_{h,rup}$ (%)	k_ε
AFRP	N-100-A1	35.5	100	200	AFRP	1	0.33	66.3	1.87	1.90	8.3	2.18	0.87
	H-100-A2	83.6	100	200	AFRP	2	0.28	113.6	1.36	1.63	5.7	1.84	0.74
	UH-100-A3	110.1	100	200	AFRP	3	0.32	154.1	1.40	1.89	6.2	1.55	0.62
AFRP	H-100-A3	85.9	100	200	AFRP	3	0.41	154.1	1.79	2.18	7.6	1.85	0.74
	UH-100-A4	110.1	100	200	AFRP	4	0.42	187.4	1.70	2.34	7.7	1.52	0.61
Filament wound AFRP	N-100-AFW	36.6	100	200	AFRP	0.3	0.48	89.2	2.44	3.15	13.7	2.24	0.77
	H-100-AFW	84.9	100	200	AFRP	0.6	0.41	169.2	1.99	2.77	9.7	2.18	0.75
	UH-100-AFW	110.1	100	200	AFRP	0.9	0.48	233.7	2.12	3.17	10.4	2.13	0.73
CFRP	N-150-C2	36.4	152	305	CFRP1	2	0.32	60.6	1.67	1.47	6.4	1.30	0.84
	H-150-C4	59.0	152	305	CFRP1	4	0.39	83.0	1.41	1.27	4.9	0.97	0.62
	UH-150-C6	102.5	152	305	CFRP1	6	0.34	131.2	1.28	1.27	4.3	0.89	0.57

Table 4. Influence of FRP type on compressive behavior of circular CFFTs

Group	Specimen	f'_{co} (MPa)	D (mm)	H (mm)	FRP type	FRP layers	f_l/f'_{co}	f'_{cc} (MPa)	f'_{cc}/f'_{co}	ε_{cu} (%)	$\varepsilon_{cu}/\varepsilon_{co}$	$\varepsilon_{h,rup}$ (%)	k_ε
UHSC AFRP & CFRP	UH-150-A4	102.2	152	305	AFRP	4	0.30	122.3	1.20	1.45	4.4	1.18	0.47
	UH-150-C5	102.5	152	305	CFRP1	5	0.29	116.0	1.13	1.04	3.1	0.81	0.52
HSC CFRP & HM CFRP	H-150-C2	59.0	152	305	CFRP1	2	0.20	66.9	1.13	1.00	3.9	1.17	0.75
	H-150-HMC2	59.0	152	305	HM CFRP	2	0.22	73.9	1.25	0.44	1.7	0.12	0.29

Table 5. Influence of tube manufacture method on compressive behavior of circular CFFTs

Specimen	f'_{co} (MPa)	D (mm)	H (mm)	FRP type	t_f (mm)	f_l/f'_{co}	f'_{cc} (MPa)	f'_{cc}/f'_{co}	ε_{cu} (%)	$\varepsilon_{cu}/\varepsilon_{co}$	$\varepsilon_{h,rup}$ (%)	k_ε
H-100-A3	85.9	100	200	AFRP	0.6	0.41	154.1	1.79	2.18	7.6	1.85	0.74
H-100-AFW	84.9	100	200	AFRP-FW	0.6	0.41	169.2	1.99	2.77	9.7	2.18	0.75

Table 6. Influence of confinement technique on compressive behavior of FRP-confined concrete

Specimen	f'_{co} (MPa)	D (mm)	H (mm)	Confinement technique	FRP type	FRP layers	f_l/f'_{co}	f'_{cc} (MPa)	f'_{cc}/f'_{co}	ε_{cu} (%)	$\varepsilon_{cu}/\varepsilon_{co}$	$\varepsilon_{h,rup}$ (%)	k_ε
N-150-A3	49.4	153	305	Tube	AFRP	3	0.46	106.3	2.15	2.96	11.9	2.32	0.93
N-150-A3W	49.4	153	305	Wrap	AFRP	3	0.46	105.9	2.14	3.06	12.3	2.24	0.90

Table 7. Influence of concrete strength on the compressive behavior of square CFFTs

Group	Specimen	Dimensions (mm)	FRP type	f'_{co} (MPa)	f_l/f'_c	f'_{cc} (MPa)	f'_{cc}/f'_{co}	ε_{cu} (%)	$\varepsilon_{cu}/\varepsilon_{co}$
Medium level of confinement	SN1	200 x 200 x 600, r: 40	CFRP1	26.7	0.50	33.8	1.27	2.39	11.2
	SH1	150 x 150 x 300, r: 30	CFRP2	76.6	0.46	81.9	1.07	1.53	5.5
	SUH1	150 x 150 x 300, r: 30	CFRP2	107.3	0.55	120.5	1.12	1.47	4.9
High level of confinement	SN2	200 x 200 x 600, r: 40	CFRP1	26.7	0.83	47.2	1.77	3.58	16.8
	SH2	150 x 150 x 300, r: 30	CFRP2	77.2	0.77	109.4	1.42	2.06	7.4
	SUH2	150 x 150 x 300, r: 30	CFRP2	110.8	0.86	146.2	1.32	1.80	5.9

Table 8. Influence of concrete strength on the compressive behavior of rectangular CFFTs

Group	Specimen	Dimensions (mm)	FRP type	f'_{co} (MPa)	f_l/f'_c	f'_{cc} (MPa)	f'_{cc}/f'_{co}	ε_{cu} (%)	$\varepsilon_{cu}/\varepsilon_{co}$
Well-rounded corners	RN1	150 x 300 x 600, r: 40	CFRP1	24.0	0.78	30.7	1.28	3.39	16.3
	RH1	113 x 225 x 300, r: 30	CFRP2	78.2	0.64	83.4	1.07	1.78	6.4
	RUH1	113 x 225 x 300, r: 30	CFRP2	110.8	0.72	102.4	0.92	1.60	5.2
Smaller corner radius	RN2	150 x 300 x 600, r: 20	CFRP1	24.0	0.78	22.2	0.93	2.93	14.1
	RH2	113 x 225 x 300, r: 15	CFRP2	78.2	0.64	59.5	0.76	1.87	6.7
	RUH2	113 x 225 x 300, r: 15	CFRP2	110.5	0.72	84.8	0.77	2.84	9.3

Table 9. Influence of internal FRP panels on compressive behavior of rectangular CFFTs

Specimen	Dimensions (mm)	FRP type	f'_{co} (MPa)	f_l/f'_c	f'_{cc} (MPa)	f'_{cc}/f'_{co}	ε_{cu} (%)	$\varepsilon_{cu}/\varepsilon_{co}$
RN3	150 x 300 x 600, r: 40	CFRP1	26.7	0.42	23.8	0.89	1.38	6.48
RN-IP	150 x 300 x 600, r: 40	CFRP1	26.7	0.42	33.0	1.24	1.81	8.50
RN-RIP	150 x 300 x 600, r: 40	CFRP1	26.7	0.42	40.7	1.52	1.72	8.08

Table 10. Influence of internal FRP tubes on compressive behavior of square CFFTs

Specimen	Dimensions (mm)	FRP type	f'_{co} (MPa)	f_l/f'_c	f'_{cc} (MPa)	f'_{cc}/f'_{co}	ε_{cu} (%)	$\varepsilon_{cu}/\varepsilon_{co}$
SN2	200 x 200 x 600, r: 40	CFRP1	26.7	0.83	47.2	1.77	3.58	16.8
SN-IT	200 x 200 x 600, r: 50	CFRP1	26.7	0.83	83.0	3.11	3.58	16.8

Figure 1. Typical circular CFFTs: from left to right, Specimens N-300-C4, N-150-C2 and N-75-C1

(a) 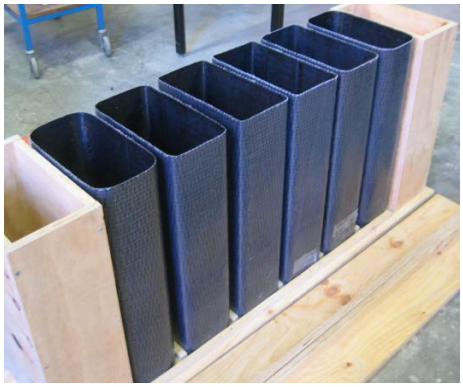

(b) 

(c) 

(d) 

Figure 2. Square and rectangular CFFTs before casting of concrete: (a) typical NSC CFFTs; (b) typical HSC and UHSC CFFTs; (c) CFFT with an internal panel; (d) CFFT with internal tubes

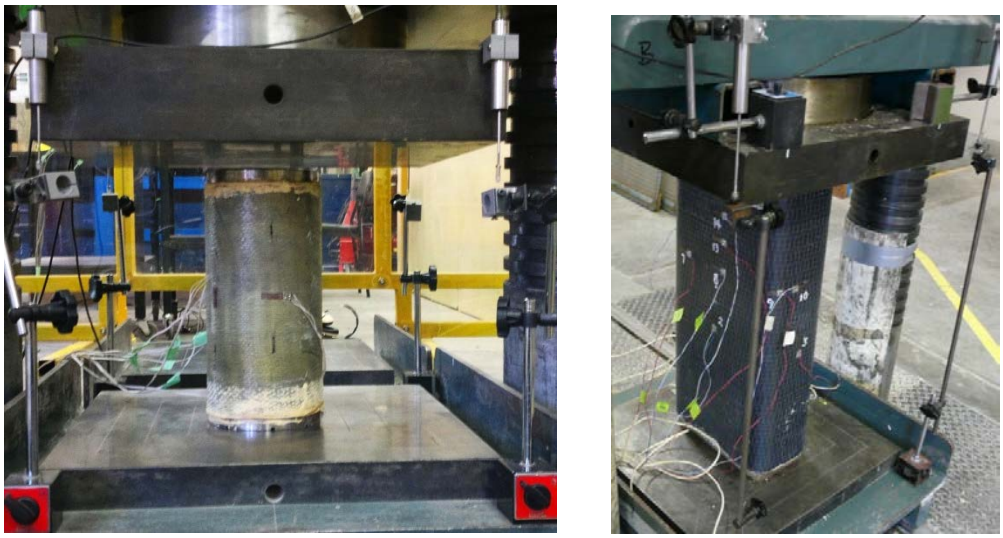

Figure 3. Test setup and instrumentation

(a)  (b) 

Figure 4. Failure modes of circular CFFTs: (a) NSC CFFT; (b) UHSC CFFT

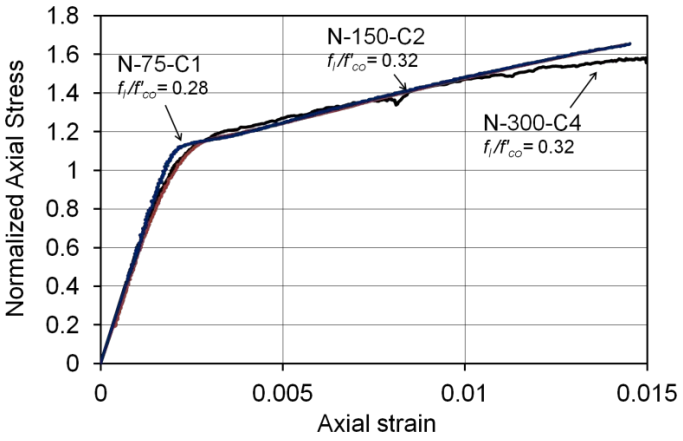

(a)

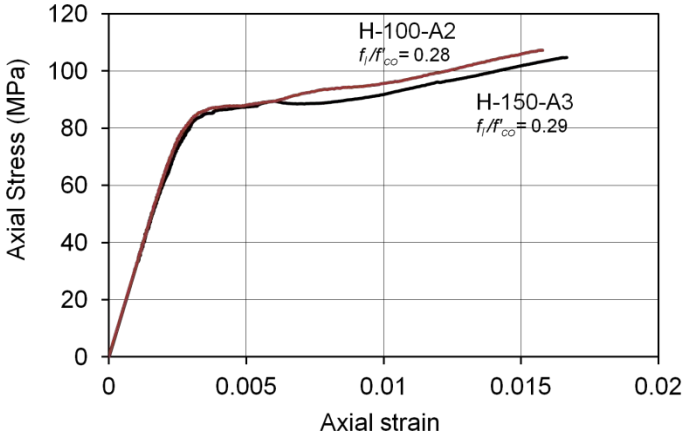

(b)

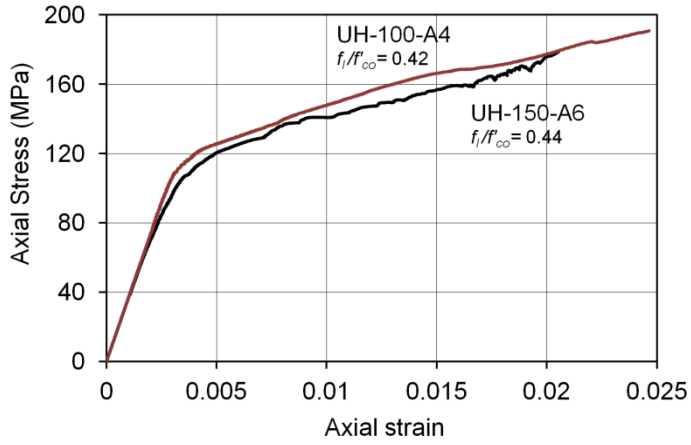

(c)

Figure 5. Influence of specimen size on compressive behavior of circular CFFTs: (a) Comparison 1: NSC; CFRP; D = 75, 150 and 300 mm; (b) Comparison 2: HSC; AFRP; D = 100 and 150 mm; (c) Comparison 3: UHSC; AFRP; D = 100 and 150 mm

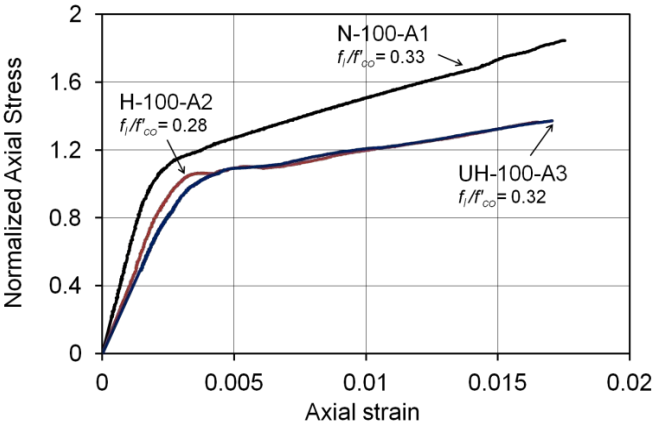

(a)

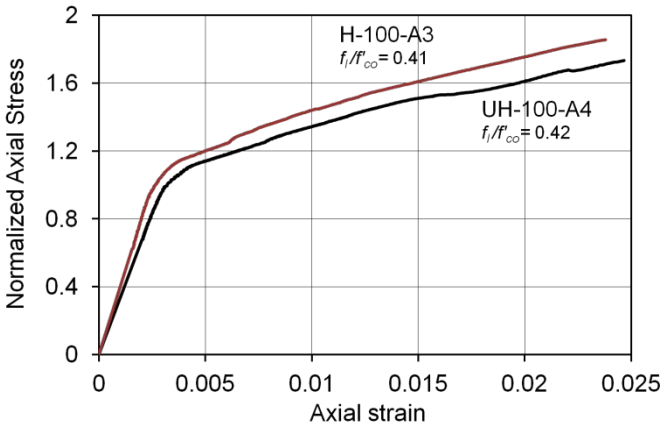

(b)

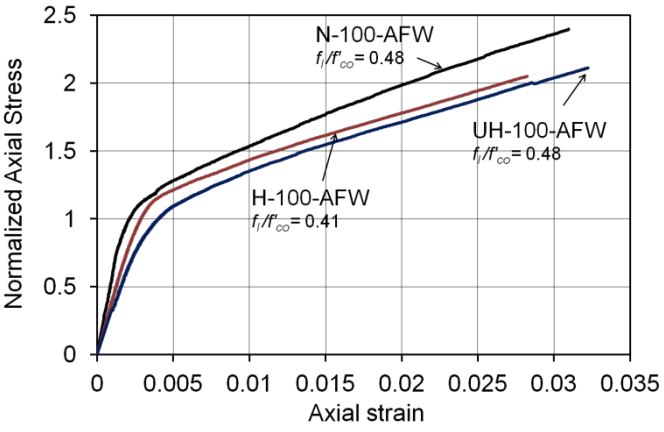

(c)

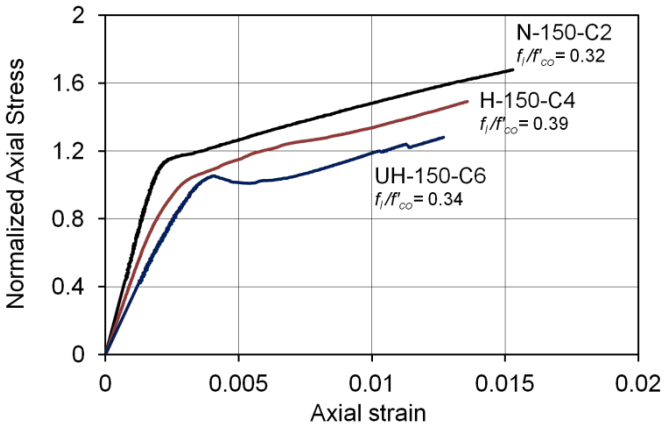

(d)

Figure 6. Influence of concrete strength on compressive behavior of circular CFFTs: (a) Comparison 1: NSC, HSC and UHSC; AFRP; D = 100 mm; (b) Comparison 2: HSC and UHSC; AFRP; D = 100 mm; (c) Comparison 3: NSC, HSC and UHSC; Filament wound AFRP; D = 100 mm; (d) Comparison 4: NSC, HSC and UHSC; CFRP; D = 150 mm

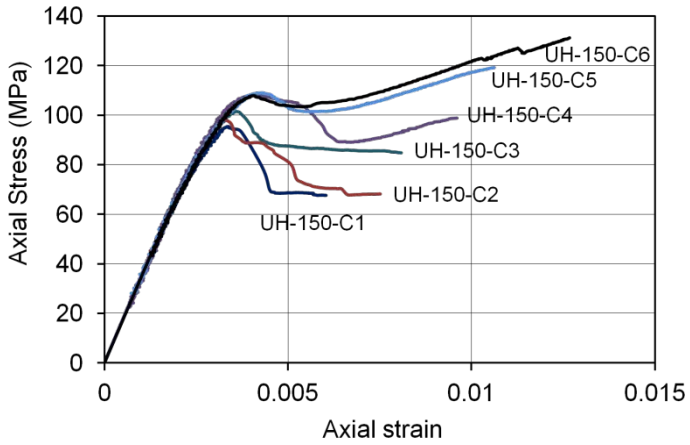

Figure 7. Influence of level of confinement on compressive behaviour of circular UHSCFFTs

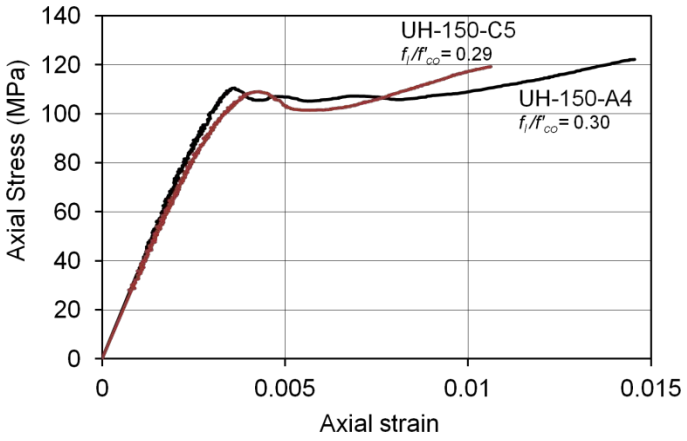

(a)

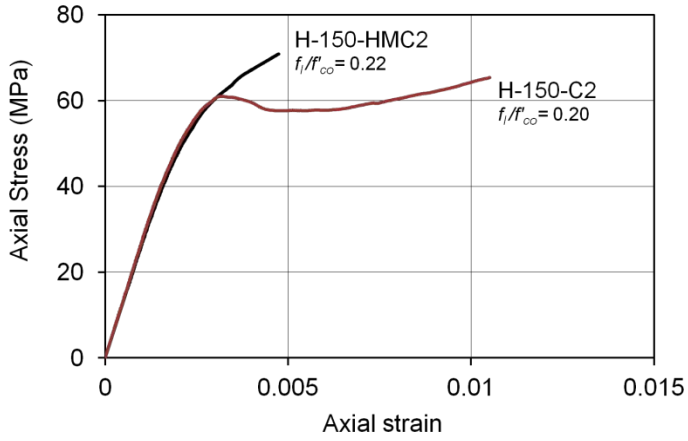

(b)

Figure 8. Influence of FRP type on compressive behavior of circular CFFTs: (a) Comparison 1: UHSC; AFRP and CFRP; D= 150 mm; (b) Comparison 2: HSC; CFRP and HM CFRP; D= 150 mm

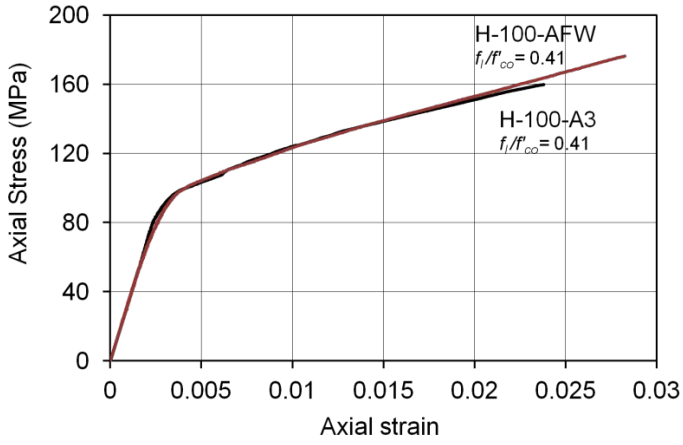

Figure 9. Influence of tube manufacturing method on compressive behavior of circular CFFTs

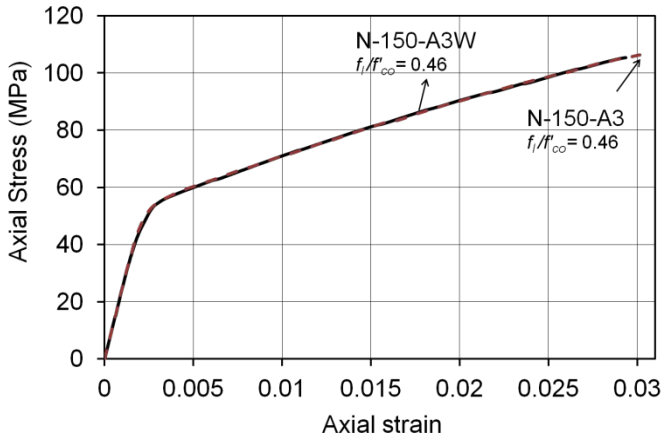

Figure 10. Influence of confinement technique on compressive behavior of FRP-confined concrete

(a)  (b)  (c) 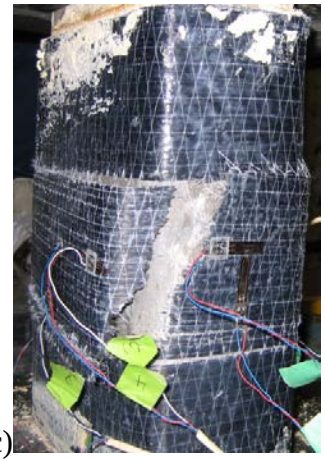

(d)  (e) 

Figure 11. Failure modes of square and rectangular CFFTs - Specimens: (a) SN2 (b) SH1 (c) RH2 (d) SUH1 (e) RUH1

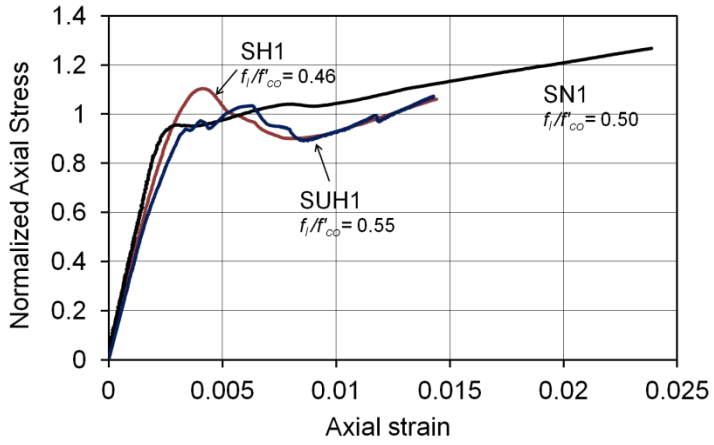

(a)

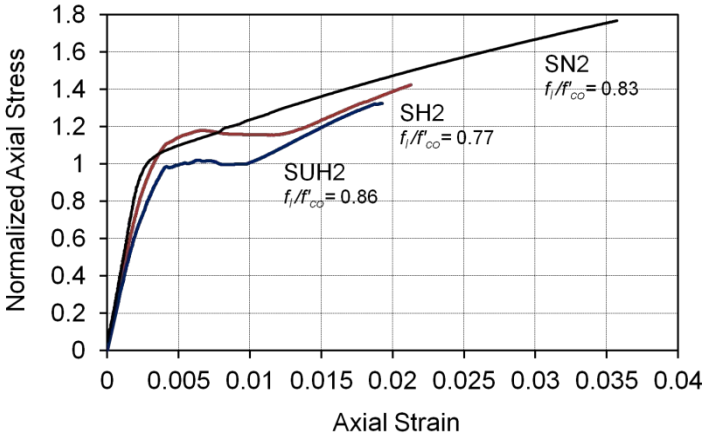

(b)

Figure 12. Influence of concrete strength on compressive behavior of square CFFTs: (a) CFFTs with medium level of confinement; (b) CFFTs with high level of confinement

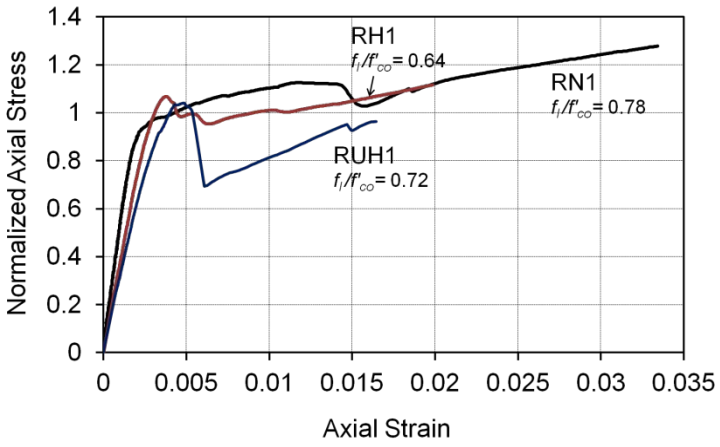

(a)

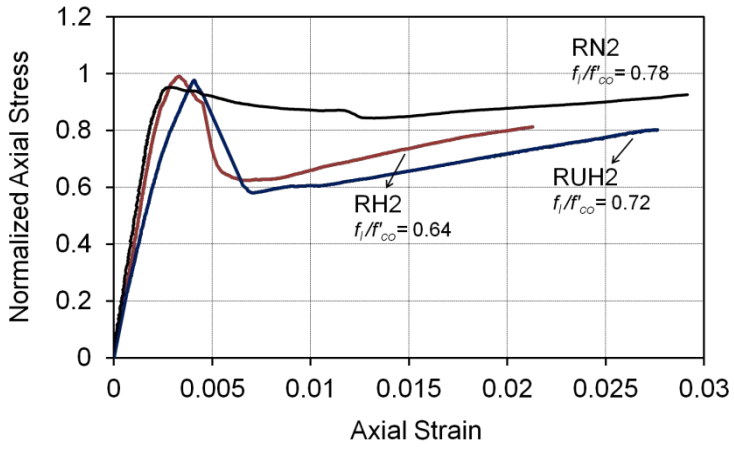

(b)

Figure 13. Influence of concrete strength on compressive behavior of rectangular CFFTs: (a) CFFTs with well-rounded corners; (b) CFFTs with smaller corner radius

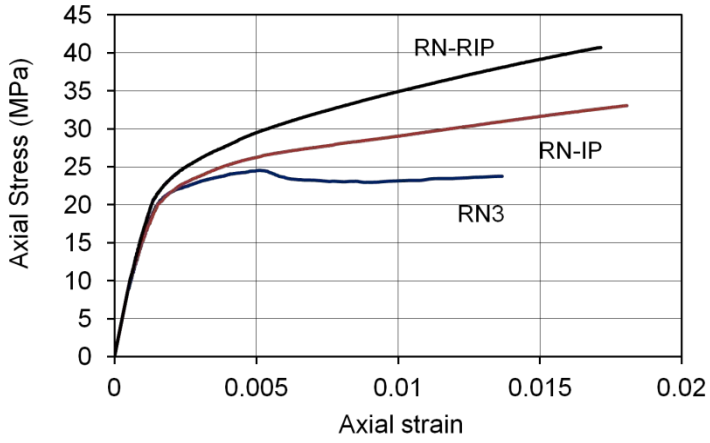

Figure 14. Influence of internal FRP panels on compressive behavior of rectangular CFFTs

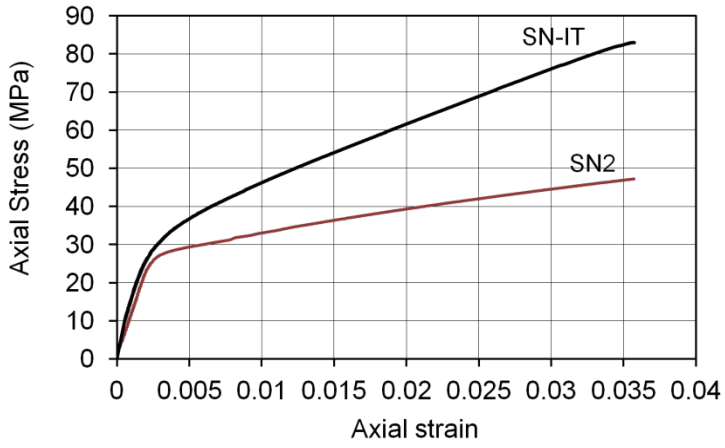

Figure 15. Influence of internal FRP tubes on compressive behavior of square CFFTs